

The *AKARI* Spectra of Luminous Infrared Galaxies in the Local Universe

HANAE INAMI,¹ HIDEO MATSUHARA,² LEE ARMUS,³ VASSILIS CHARMANDARIS,^{4,5} TANIO DÍAZ-SANTOS,⁶
JASON SURACE,³ SABRINA STIERWALT,^{7,8} AND GOALS TEAM⁹

¹Univ Lyon, Univ Lyon1, Ens de Lyon, CNRS, Centre de Recherche Astrophysique de Lyon (CRAL) UMR5574, F-69230, Saint-Genis-Laval, France

²Institute of Space and Astronautical Science, Japan Aerospace Exploration Agency, 3-1-1 Yoshinodai, Chuo, Sagami-hara, Kanagawa 252-5210, Japan

³Infrared Processing and Analysis Center, MC 314-6, Caltech, 1200 E. California Blvd., Pasadena, CA 91125, USA

⁴Institute for Astronomy, Astrophysics, Space Applications & Remote Sensing, National Observatory of Athens, GR-15236, Penteli, Greece

⁵University of Crete, Department of Physics, GR-71003, Heraklion, Greece

⁶Núcleo de Astronomía de la Facultad de Ingeniería, Universidad Diego Portales, Av. Ejército Libertador 441, Santiago, Chile

⁷Department of Astronomy, University of Virginia, P.O. Box 400325, Charlottesville, VA 22904, USA

⁸National Radio Astronomy Observatory, 520 Edgemont Road, Charlottesville, VA 22903, USA

⁹<http://goals.ipac.caltech.edu/>

ABSTRACT

We have combined *AKARI* 2.5–5 μm and *Spitzer* 5.2–38 μm spectra of 145 local luminous infrared galaxies (LIRGs) drawn from the Great Observatories All-sky LIRG Survey (GOALS). The equivalent widths (EQWs) of the polycyclic aromatic hydrocarbon (PAH) emission features detected at 3.3 μm and 6.2 μm , the two most commonly used indicators for classifying the central energy sources (starburst or active galactic nucleus, AGN), do not appear to be linearly correlated. Moreover, about 30% of the AGN-dominated galaxies classified by the 3.3 μm PAH EQW are, on the contrary, suggested to be starburst-dominated galaxies by the 6.2 μm PAH EQW. We find that the *Spitzer* spectra of the sources with low 3.3 μm PAH EQW but high 6.2 μm PAH EQW are remarkably similar to the spectra of pure starburst sources. However, their 2–5 μm continua in *AKARI* spectra are much bluer, suggesting that the continuum is dominated by stellar emission rather than hot dust emission. Based on these results, we suggest a revised diagnostic using the 3.3 μm PAH EQW and the continuum color. We also report on a possible diagnostic with the capabilities of the *James Webb Space Telescope* (*JWST*) based on the results from the *AKARI* and *Spitzer* data.

Keywords: galaxies: active — galaxies: starburst — infrared: galaxies

1. INTRODUCTIONS

The *AKARI* infrared satellite (Murakami et al. 2007) covers the 2.5–5 μm region of the infrared spectrum, where *Spitzer* is not able to observe. In this wavelength range, hot dust (~ 1000 K) emission, which is due to AGN, and PAH emission features, which are a direct probe of star formation, can provide a reliable selection of starburst/AGN dominated galaxies. When *JWST* is launched, the only observable PAH features at $z > 3.5$ will be the 3.3 μm feature.

We targeted a subset of the local LIRGs in the GOALS sample (Armus et al. 2009). Our target galaxies are likely to be the best local analogs of high- z active galaxies, which dominate the star formation rate density at $z \sim 2$ –3, the peak era of galaxy formation in the Universe (e.g., Madau & Dickinson 2014).

In this proceedings, we aim at characterizing the starburst/AGN diagnostic features of PAH and hot dust emission in the infrared based on a large LIRG sample in the local Universe. We also report on possible diagnostics with *JWST* for galaxies at $z = 0$ –1.5.

2. OBSERVATIONS AND DATA REDUCTION

Out of 202 LIRG systems in the GOALS sample, 145 nuclei were observed with the *AKARI* Infrared Camera (IRC; Onaka et al. 2007) using the pointed spectroscopic mode (2.5–5 μm) with the Np aperture ($1' \times 1'$). The observations were carried out between 2006 October 29 and 2010 February 14.

We used the standard data reduction software package (IRC Spectroscopy Toolkit for Phase 3, Version 20101025) to perform dark subtraction, linearity correction, flat correction, background subtraction, wavelength calibration, spectral

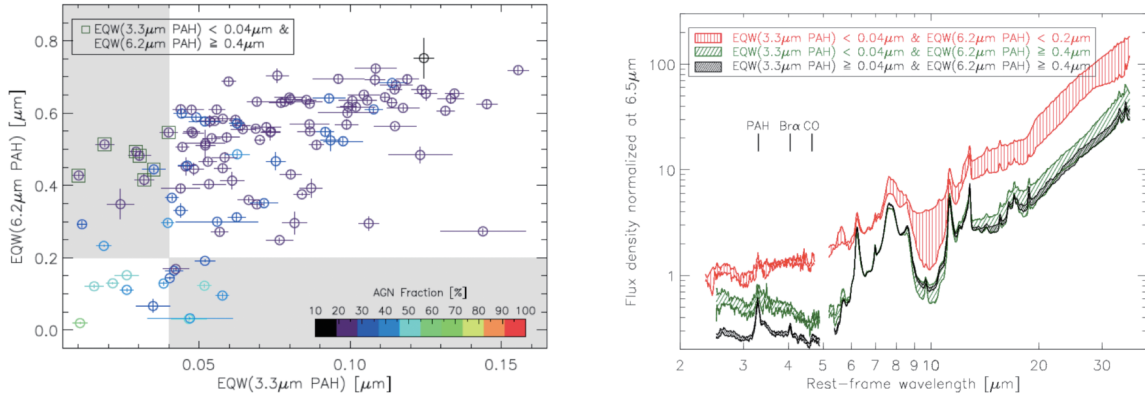


Figure 1. [Left] Comparison of 6.2 μm PAH EQW and 3.3 μm PAH EQW. The colors of the symbols indicate the AGN bolometric fraction as shown in the color bar at bottom right. The green squares represent the objects with EQW(3.3 μm PAH) < 0.04 μm and EQW(6.2 μm PAH) ≥ 0.4 μm. [Right] The median spectra of our local LIRG samples classified by 3.3 μm and 6.2 μm PAH EQWs as indicated in the figure.

inclination correction, and spectral response calibration. The 1D spectra were extracted with an aperture width of 4'4 (3 pixels), which is similar in size to the slit width of the *Spitzer* IRS Short-wavelength Low-resolution (SL) spectroscopy. We combine the *AKARI* spectra and the *Spitzer* spectra to investigate spectral properties in the 2.5–38 μm range.

We also adopt the mean of the bolometric AGN fraction (“AGN fraction”) to denote the AGN contribution to the total bolometric luminosity (Table 2 in Díaz-Santos et al. 2017), based on multiple AGN indicators in the mid-infrared from the *Spitzer*/IRS data: [Ne v]/[Ne II] (Inami et al. 2013), [O IV]/[Ne II] (Inami et al. 2013), 6.2 μm PAH EQW (Stierwalt et al. 2013), $S_{30\mu\text{m}}/S_{15\mu\text{m}}$ (Stierwalt et al. 2013), and the Laurent diagram (Laurent et al. 2000; Petric et al. 2011).

3. RESULTS AND DISCUSSION

3.1. Starburst/AGN Diagnostics with PAH Features

The PAH features are the most widely used mid-infrared spectral features for distinguishing starburst- and AGN-dominated sources. In the *AKARI* spectral range, sources with EQWs of 3.3 μm PAH below 0.04 μm are typically classified as AGN dominated (e.g., Moorwood 1986; Imanishi et al. 2010). In the *Spitzer* spectral range, EQWs of 6.2 μm PAH smaller than 0.2 μm are often considered to indicate AGN dominated (e.g., Armus et al. 2007; Petric et al. 2011).

In Figure 1 (left), we directly compare the 3.3 μm and 6.2 μm PAH EQWs. No linear correlation is found between them. Instead, a wide dispersion is detected in the 3.3 μm PAH EQWs of galaxies with 6.2 μm PAH EQW higher than ~ 0.6 μm, which is the typical value for pure starburst galaxies. This scatter in 3.3 μm PAH EQW decreases with decreasing 6.2 μm PAH EQW. However, galaxies with 3.3 μm PAH EQW < 0.04 μm do not show a decreasing 6.2 μm PAH EQW but a large scatter in their 6.2 μm PAH EQWs (the top left gray region). About 1/3 of these galaxies even reach the starburst dominated criterion based on their 6.2 μm PAH EQWs, whereas the 3.3 μm PAH EQWs imply that they are AGN dominated.

It is unlikely that the dust emission from an AGN dominates the 2–5 μm range but does not contribute significantly to the mid-infrared ($T \sim 500$ K), given their intrinsically red, power-law continuum emission (Weedman et al. 2005; Armus et al. 2007). This contradiction between the low 3.3 μm and high 6.2 μm PAH EQWs may be attributed to (1) an absence of small PAH grains, (2) a larger fraction of ionized PAH grains, or (3) an excess of stellar emission at $\lambda \lesssim 5$ μm.

The relative strengths of the different PAH bands vary with the grain size and the ionization state of PAH (Draine & Li 2001; Li & Draine 2001; Draine & Li 2007; Tielens 2008). We use the flux ratio-ratio diagram of PAH(11.3 μm)/PAH(7.7 μm) vs. PAH(6.2 μm)/PAH(7.7 μm) as in Draine & Li (2001) to examine where the sources with low 3.3 μm but high 6.2 μm PAH EQWs lie compared with the entire sample. The sources with the low 3.3 μm but high 6.2 μm PAH EQWs are distributed over a wide range of the grain size and ionization state without any obviously biased distributions compared to the other sources. In addition, these sources do not show particularly weak 3.3 μm PAH emission relative to 6.2 μm PAH emission. Therefore, the fact that they have low 3.3 μm and high 6.2 μm PAH EQWs is related to the continuum properties, not the PAH properties.

Next, we investigate the 6.2 μm PAH EQW versus the *AKARI* 2.5–5 μm continuum slope. With one exception, all of the galaxies with relatively blue continuum slopes suggested by the flux density ratios of $F_{\nu}(4.3 \mu\text{m})/F_{\nu}(2.8 \mu\text{m}) \lesssim 1$ display PAH(6.2 μm) EQW > 0.2 μm, but galaxies with PAH(6.2 μm) EQW < 0.4 μm show progressively redder continuum slopes with decreasing 6.2 μm PAH EQWs. Interestingly, all of the sources with low 3.3 μm but high 6.2 μm PAH EQWs have $F_{\nu}(4.3 \mu\text{m})/F_{\nu}(2.8 \mu\text{m}) < 1$, bluer than most of the pure starburst LIRGs with PAH(6.2 μm) EQW > 0.4 μm.

The blue continuum of the sources with low 3.3 μm but high 6.2 μm PAH EQWs can also be identified in Figure 1 (right). For galaxies with PAH(6.2 μm) EQW ≥ 0.4 μm (green and black), although the sources with low PAH(3.3 μm) EQW show a bluer continuum in the *AKARI* wavelength range, interestingly, the *Spitzer* spectra are mostly identical regardless of their PAH(3.3 μm) EQWs.

THE AKARI SPECTRA OF LOCAL LIRGS

O37 - 3

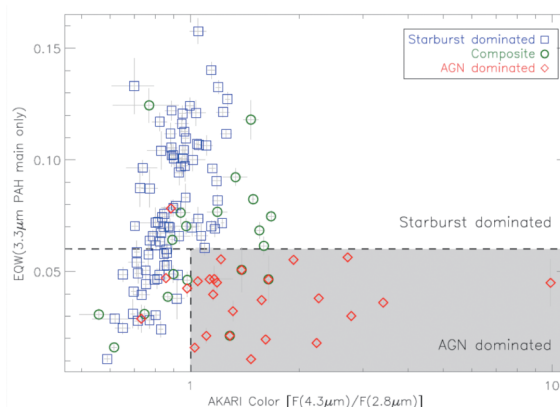


Figure 2. Proposed revised starburst/AGN diagnostics based on the *AKARI* 2.5–5 μm data. The blue squares and red diamonds indicate the starburst- and AGN-dominated galaxies, respectively. The green circles are the composite of the two.

Based on these results, we propose the following two scenarios to explain the inconsistency between the 3.3 μm and 6.2 μm PAH EQWs for the starburst/AGN classification (low 3.3 μm but high 6.2 μm PAH EQWs). The evolutionary stage of these galaxies is such that (1) although they are still actively forming stars, the stellar populations have aged enough since the onset of star formation, such that the near-infrared continuum is no longer dominated by hot dust (either from an AGN or ultra-compact starbursts) but rather by the stellar continuum of red super-giants or asymptotic giant branch stars (with ages of a few tens of Myr), or (2) what we are witnessing is a nascent starburst which dominates the mid-infrared emission, while the near-infrared continuum is tracing the underlying, old population of stars that were already formed long before the current burst of star formation. Both of these explanations are plausible and do not conflict with each other if the ionized gas is deeply obscured and cannot be observed.

3.2. Revised *AKARI* Starburst/AGN Diagnostic

Based on the additional information provided by the *Spitzer*/IRS data, we propose a revision of the commonly used starburst/AGN diagnostic as shown in Figure 2. This diagnostic employs the 3.3 μm PAH EQW and the 2–5 μm continuum slope, Γ , which we measure as the flux density ratio, $F_{\nu}(4.3 \mu\text{m})/F_{\nu}(2.8 \mu\text{m})$. We prefer the flux ratio because Γ requires fitting the continuum slope (Imanishi et al. 2010; Lee et al. 2012). While many previous studies have also used similar limits on the 3.3 μm PAH EQW or the continuum slope, these two selection criteria are used independently. We claim instead that both of them must be fulfilled because we discovered as much as 1/3 of our local LIRG sample with $\text{PAH}(3.3 \mu\text{m}) \text{EQW} < 0.04 \mu\text{m}$ can be misclassified as AGN.

3.3. Starburst/AGN Diagnostics with *JWST*

We also measured the J , H , and K_S -band fluxes of our sample based on the imaging data from the Two Micron All Sky Survey (2MASS) to widen the spectral coverage to 1–38 μm of our infrared spectra of individual local LIRGs. Taking advantage of having this wide spectral coverage of a large sample, we explore possible starburst/AGN diagnostics with *JWST* photometric filters in the redshift range of 0–1.5 by manually redshifting the spectra to higher redshifts.

The color-color diagram of F770W/F444W vs. F560W/F356W is shown in Figure 3, which mimics the *Spitzer*/IRAC selection of AGN (Lacy et al. 2004; Donley et al. 2012). These *JWST* broadband filters are selected to be closest to the IRAC filters. The evolution in the colors is clearly seen: AGN-dominated galaxies mostly stay within the AGN selection boundaries up to $z = 1.5$, while starburst-dominated galaxies become bluer in both of the colors from $z = 0$ to 0.3. At higher redshifts, starburst-dominated galaxies remain within the bottom left region of the Lacy et al. (2004) boundaries and cannot be separated from the AGN-dominated galaxies with this color-color diagram. On the other hand, the boundaries of Donley et al. (2012) give a cleaner selection as expected. This trend agrees well with the results of Donley et al. (2012), that pure starburst galaxies become bluer at least up to $z \sim 1.5$ and lie on the bottom left side just outside of the AGN selection boundaries. For this color-color selection, $z = 1.5$ is the redshift limit for the wavelength coverage of our spectral energy distributions (SEDs), because the blue-end of the SEDs (2MASS J -band) shift out from the coverage of F356W.

4. SUMMARY

We presented the investigation of the combined *AKARI* and *Spitzer* spectra of 145 local LIRG nuclei of the GOALS sample. Based on the spectral features detected in the combined spectra, we found that:

- No linear correlation is seen between 3.3 μm and 6.2 μm PAH EQWs. About 1/3 of the sources with low 3.3 μm PAH EQW ($< 0.04 \mu\text{m}$, indicating AGN) have high 6.2 μm PAH EQW ($\geq 0.4 \mu\text{m}$, indicating starbursts). Their 2–5 μm continuum is dominated by stellar emission rather than hot dust due to AGN.

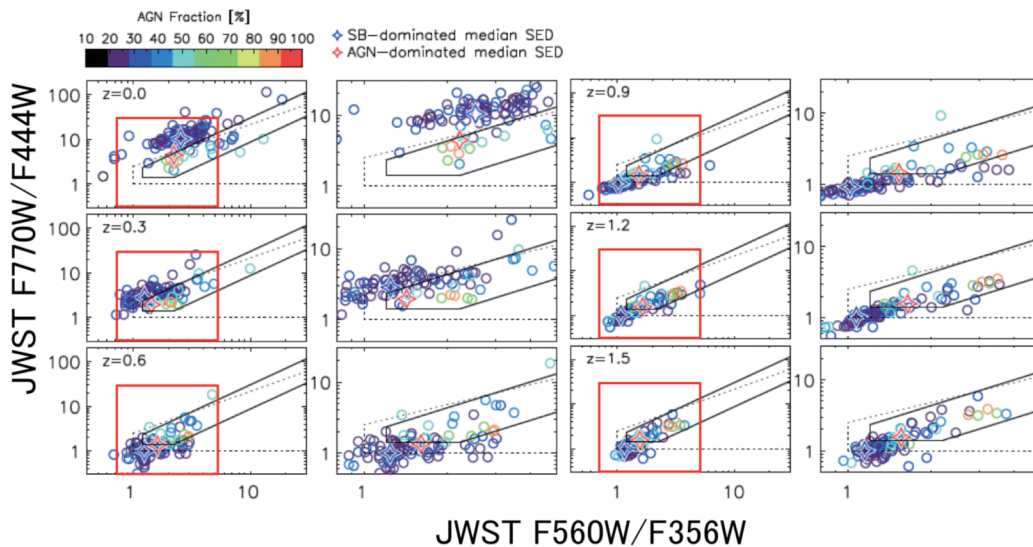


Figure 3. AGN color-color selection with the *JWST* photometric filters from $z = 0.0$ (top left) to $z = 1.5$ (bottom right). The red boxes in each panel denote the zoomed-in plot shown in the panel on the right of it. The circular symbols are individual galaxies and their colors indicate the AGN bolometric fraction as shown in the color bar at top left. The blue and red stars represent the flux ratios measured in the median SEDs of starburst- and AGN-dominated galaxies. The solid and dashed lines are taken from Donley et al. (2012) and Lacy et al. (2004), respectively.

- The $2\text{--}5\ \mu\text{m}$ continuum slope is essential in order to cleanly select AGN-dominated galaxies with $3.3\ \mu\text{m}$ PAH EQW.
- The color-color diagram of F770W/F444W vs. F560W/F356W of the *JWST* photometric filters is effective in selecting AGN at least up to $z = 1.5$ using the same conditions as Donley et al. (2012).

ACKNOWLEDGMENTS

This research is based on observations with *AKARI*, a JAXA project with the participation of ESA. The *Spitzer* Space Telescope is operated by the Jet Propulsion Laboratory, California Institute of Technology, under NASA contract 1407. This research has made use of the NASA/IPAC Extragalactic Database (NED) and the Infrared Science Archive (IRSA) which are operated by the Jet Propulsion Laboratory, California Institute of Technology, under contract with the National Aeronautics and Space Administration.

REFERENCES

- Armus, L., Charmandaris, V., Bernard-Salas, J., et al. 2007, *ApJ*, 656, 148
 Armus, L., Mazzarella, J. M., Evans, A. S., et al. 2009, *PASP*, 121, 559
 Díaz-Santos, T., Armus, L., Charmandaris, V., et al. 2017, *ApJ*, 846, 32
 Donley, J. L., Koekemoer, A. M., Brusa, M., et al. 2012, *ApJ*, 748, 142
 Draine, B. T. & Li, A. 2001, *ApJ*, 551, 807
 Draine, B. T. & Li, A. 2007, *ApJ*, 657, 810
 Imanishi, M., Nakagawa, T., Shirahata, M., Ohyama, Y., & Onaka, T. 2010, *ApJ*, 721, 1233
 Inami, H., Armus, L., Charmandaris, V., et al. 2013, *ApJ*, 777, 156
 Lacy, M., Storrie-Lombardi, L. J., Sajina, A., et al. 2004, *ApJS*, 154, 166
 Laurent, O., Mirabel, I. F., Charmandaris, V., et al. 2000, *A&A*, 359, 887
 Lee, J. C., Hwang, H. S., Lee, M. G., Kim, M., & Lee, J. H. 2012, *ApJ*, 756, 95
 Li, A. & Draine, B. T. 2001, *ApJ*, 554, 778
 Madau, P. & Dickinson, M. 2014, *ARA&A*, 52, 415
 Moorwood, A. F. M. 1986, *A&A*, 166, 4
 Murakami, H., Baba, H., Barthel, P., et al. 2007, *PASJ*, 59, 369
 Onaka, T., Matsuhara, H., Wada, T., et al. 2007, *PASJ*, 59, 401
 Petric, A. O., Armus, L., Howell, J., et al. 2011, *ApJ*, 730, 28
 Stierwalt, S., Armus, L., Surace, J. A., et al. 2013, *ApJS*, 206, 1
 Tielens, A. G. G. M. 2008, *ARA&A*, 46, 289
 Weedman, D. W., Hao, L., Higdon, S. J. U., et al. 2005, *ApJ*, 633, 706